https://doi.org/10.1016/j.istruc.2023.105651
This is the Pre-Published Version.

Mechanical properties of corner material in cold-formed steel structure: from normal strength to high strength

Haixin Liu [a], Junbo Chen [b, *], Tak–Ming Chan [a, c]

[a] Department of Civil and Environmental Engineering, The Hong Kong Polytechnic University, Hung Hom, Hong Kong, China

[b] School of Civil and Hydraulic Engineering, Huazhong University of Science and Technology, Wuhan, Hubei, China

[c] Chinese National Engineering Research Centre for Steel Construction (Hong Kong Branch), The Hong Kong Polytechnic University, Hung Hom, Hong Kong, China

*Corresponding author: junbochen@hust.edu.cn

Abstract:

Cold-forming effect varies from normal strength steel to high strength steel due to the different chemical compositions and mechanical properties of parent materials. To date, research studies on material characterisation of cold–formed steels have been mainly focusing on the normal strength structural steel, while systematic research on high strength structural steel remains scarce. In this paper, an experimental investigation into changes in mechanical properties of high strength steel undergoing various levels of plastic deformation is firstly presented. The test results have been combined with other available high strength steel data, and compared to the normal strength steel data. Of the analysis results indicated, unified predictive equations, modified from Karren's model in 1967 can predict the strength enhancement behaviours of normal strength and high strength steel, utilising the ultimate-to-yield strength ratio of parent materials $f_{u,f}/f_{y,f}$ and inner radius-to-thickness ratio after cold–forming r_i/t. Moreover, the decreases in the Young's modulus, ultimate strain and elongation at fracture of normal strength and high strength steel after cold-forming can be predicted with no further grouping required. Statistical evaluation results confirm the accuracy of the proposed

© 2023. This manuscript version is made available under the CC-BY-NC-ND 4.0 license http://creativecommons.org/licenses/by-nc-nd/4.0/

predictive expressions. This paper extends the scope of the strength enhancement equation in current north American cold-formed steel design code AISI S100-16 to high strength steels with grade up to 960 MPa, and provides key predictive material equations that can be further used in the design or numerical modelling of cold-formed steel structures.

Keywords: Predictive models; Cold–formed steels; Mechanical properties; Strength enhancement; Normal strength steel; High strength steel.

1. Introduction

With the advancement of steel manufacturing methods like thermal–mechanical controlled processing (TMCP) and quenching and tempering (QT), the high strength structural steel (HSS) with nominal yield strength no less than 460 MPa are now commercially available in the markets. HSS has been increasingly used in the construction industry, as the higher strength–to–weight ratio of HSS results in reduced component sizes [1], and in the saving of energy and raw materials [2]. Compared to the normal strength steel (NSS), the higher carbon content and the intervention of other alloys in HSS achieve a higher yield strength but relatively lower ductility. Thus, the nature of HSS may alter the strain hardening and ageing behaviours during the cold–forming process. As illustrated in Fig. 1 [3], the strain hardening effect generally leads to a reduced Young's modulus and increased proportional limit strength, but does not affect the ultimate tensile strength and the ductility [4], whilst the strain aging effect may result in enhanced yield and ultimate strengths, but deteriorated ductility [5], as compared with the mechanical properties of parent materials.

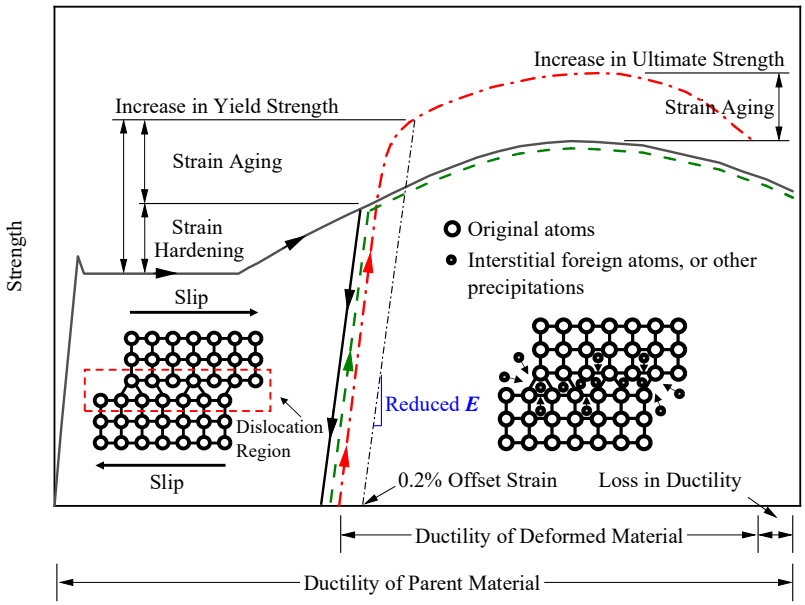

Fig. 1. Effects of strain hardening and strain aging [3].

Due to the advantages of the great flexibility of customised cross-sectional profiles, the high strength–to–weight ratio, and the ease of fabrication and installation, the applications of cold–formed steel are extensively adopted in structural members like column [6, 7], beam [8, 9], truss member [10], and flooring systems [11]. For NSS, Karren [12] first conducted a comprehensive investigation on the enhanced yield strength after cold–forming, covering the measured yield strength of parent materials from 212 MPa to 295 MPa. Karren adopted a power equation to represent the strain hardening behaviour of the plastic region in true stress–strain response (σ_T–ε_T), as given in Eq. (1):

$$\sigma_T = k\left(\varepsilon_T\right)^{n_{se}} \tag{1}$$

in which k and n_{se} are the material coefficient and strain–hardening exponent, respectively. Incorporating the power law equation and assuming a simplified corner analysis model, predictive expression of the enhanced yield strength $f_{y,c}$ for the corner material was proposed and it was further standardised in American cold–formed steel members design specification [13] and Australian cold–formed steel structures design standard [14], with a rewritten form as expressed in Eq. (2).

$$f_{y,c}=\frac{B_c f_{y,f}}{\left(r_i/t\right)^{\beta}} \text{ in which } \begin{cases} B_c=3.69\left(f_{u,f}/f_{y,f}\right)-0.819\left(f_{u,f}/f_{y,f}\right)^2-1.79 \\ \beta=0.192\left(f_{u,f}/f_{y,f}\right)-0.068 \end{cases} \quad (2)$$

in which $f_{y,f}$ and $f_{u,f}$ are the yield and ultimate strengths of the parent material, r_i is the inner radius of the cold-formed corner, and t is the plate thickness. This model suggests that the enhanced yield strength at the corners is related to the $f_{u,f}/f_{y,f}$ ratio of parent materials and the r_i/t ratio, which is an indicator of plastic deformation experienced in the corner.

Abdel–Rahman and Sivakumaran [15] and Cruise and Gardner [16] found that for cold–formed sections fabricated from different manufacturing processes, the enhanced strength extends from the corner region to the section flat face in various degrees, and they modified Karren's predictive expression accordingly based on their experimental results. Gardner et al. [17] found that Eq. (2) provided unconservative predictions for the strength enhancement of corner materials in cold–rolling NSS hollow sections, which experienced a particular, two–stage strain development history. On the basis of the collected database comprising 40 corner test results, Gardner et al. [17] modified the coefficients of Karren's predictive expression to have a better prediction result for cold–rolling NSS hollow sections. More recently, a comprehensive experimental investigation into the cold–forming effects of NSS was conducted by Liu et al. [3], covering a wide range of material parameters ($f_{y,f}$ ranging from 282 MPa to 432 MPa and $f_{y,c}$ after cold–forming varying from 351 MPa to 625 MPa) and various geometric profiles of press–braked angles (r_i/t ranging from 0.6 to 7.6 and included angle varying from 90° to 150°). Based on 241 collected corner coupon data extracted from both of cold–rolling and press–braking sections, a series of predictive expressions were proposed to predict the increase of yield and ultimate strengths and loss in ultimate strain and elongation at fracture in the corner regions of cold–formed NSS structures.

By determining the induced plastic strains during the fabrication process and harnessing the parent material parameters, Rossi et al. [18] proposed an alternative model to predict the enhanced

yield strength for any structural sections cold–formed from non–linear metallic materials, as given from Eq. (3) to Eq. (6).

$$f_{\mathrm{y,c}} = p\left(\varepsilon_{\mathrm{c,av}} + \varepsilon_{0.2}\right)^{q} \text{, but} f_{\mathrm{y,c}} \text{„} \ f_{\mathrm{u,f}} \tag{3}$$

$$\varepsilon_{\mathrm{c,av}} = \frac{t}{2\left(2r_{\mathrm{i}} + t\right)} \tag{4}$$

$$p = \frac{f_{\mathrm{y,f}}}{\varepsilon_{0.2}^{q}} \tag{5}$$

$$q = \frac{\ln\left(f_{\mathrm{y,f}} / f_{\mathrm{u,f}}\right)}{\ln\left(\varepsilon_{0.2} / \varepsilon_{\mathrm{u,f}}\right)} \tag{6}$$

where $\varepsilon_{\mathrm{c,av}}$ is the averaged plastic strain induced in the corner region, p and q are material parameters obtained directly from the mechanical properties of parent material, $\varepsilon_{0.2}$ equals $0.002+f_{\mathrm{y,f}}/E_{\mathrm{f}}$, and $\varepsilon_{\mathrm{u,f}}$ is the ultimate strain of parent material. However, in this model, to avoid a lengthy pre–determination process of material parameters, a simple power law model with a similar form of Eq. (1) was adopted to represent the stress–strain response of parent materials. To some content, this procedure may compromise the final prediction accuracy. Rasmussen and Hancock [19] and Dubina et al. [20] presented that it is of significance to determine the increasing strength in cold–formed steel structures resulting from the cold–forming effect. Moreover, in terms of the overall cross–section resistance, the inclusion of strength enhancement of cold–formed corners was recommended in current international codes [13, 14, 21].

In terms of HSS, Pham et al. [22] conducted an investigation on the effect of the fabrication process on microstructure and mechanical properties of cold–formed high strength G450 channel sections, and proposed a recommended modification for Eq. (2) to predict better the enhanced corner yield strength of this specific steel material. Based on the test results of 30 corner coupons extracted from irregular hexagonal hollow sections, Liu et al. [23] proposed a modified Karren's predictive expression to predict the enhanced yield strength of Q690 HSS accurately. Xiao [24] found that after

106 cold–forming of S690 square hollow sections, if r_i/t was so tight that the induced plastic deformation
107 exceeded the deformation limit of parent materials, the waving and cracking may occur on both
108 surfaces of the corner. It may be basically attributed to the relatively lower $f_{u,f}/f_{y,f}$ ratio of HSS, which
109 results in a lower material ductility and reflects a lower potential of cold–work. Similar finding of
110 enhanced yield strength in corners of cold–formed structural sections can be found in [25-27] for
111 S700, S900 and S960 HSSs, respectively. It can be concluded from these literature that studies on the
112 cold–forming effect of HSS were quite scattered and discrete, and a study into the continuous
113 development of cold–forming effect under different level of induced plastic deformation was still
114 lacking. Furthermore, whether the predictive expressions for enhanced yield strength can be extended
115 to HSS is still unknown, since those models were developed based on limited test data.

116 For specific scenarios such as advanced numerical modelling and extensive parametric studies of
117 cold–formed steel structures, a precise description of material stress–strain response is crucial.
118 Following the need for more accurate material stress–strain relationships, Quach and Huang [28] and
119 Gardner and Yun [29] both developed two–stage Ramberg–Osgood models to describe the rounded
120 stress–strain curves of cold–formed steels. To precisely generate stress–strain curves through these
121 material constitutive models, the adopted key material parameters, such as the Young's modulus, yield
122 strength, ultimate strength, and ultimate strain, should be carefully selected. However, to date, these
123 key material parameters of cold–formed steels in the corner region can only be acquired through the
124 experimental test, making it inconvenient when applying these material constitutive models.

125 To address these research gaps, a consistent and thorough material test was first conducted to
126 investigate the cold–forming effects of HSS in this research. A total of 12 flat coupons machined from
127 parent materials (Q460, Q550, and Q690 HSSs) and 68 corner coupons extracted from cold–formed
128 angle sections with a spectrum of r_i/t ratios (0.73 – 5.63) and included angles θ (90° – 150°) were

tested. Subsequently, the obtained test results were combined with the data collected from global literature to develop an extensive experimental database covering normal to high strength structural steel. Based on the large set of data comprising 341 flat coupons and 613 corner coupon results, Young's moduli, enhanced yield and ultimate strengths, loss in ultimate strain and elongation at fracture between NSS and HSS after cold–forming were compared, and corresponding predictive expressions were proposed.

2. Experimental investigation

To further study the changes in mechanical properties of HSS after cold–forming, an experimental investigation was carried out on four different high strength structural steel plates, namely 3 mm Q460, 6 mm Q460, 6 mm Q550, and 3 mm Q690 plates. Different amounts of plastic deformation were achieved through press–braking the parent material into different included angles using various punches (in different punch radii). Chemical compositions of the investigated steel plates are reported in Table 1.

Table 1. Chemical compositions reported in mill certificates.

Steel plate	Chemical composition (%)											
–	C	Si	Mn	P	S	Al	Nb	Ni	Cr	Ti	V	CEV
Q460 – 3 mm	0.07	0.07	1.49	0.008	0.001	–	0.022	–	–	0.01	0.001	0.35
Q460 – 6 mm	0.07	0.05	1.51	0.015	0.001	–	0.021	–	–	0.01	0.001	0.34
Q550 – 6 mm	0.07	0.07	1.56	0.009	0.004	0.027	–	–	–	0.12	0.003	0.33
Q690 – 3 mm	0.06	0.06	1.83	0.014	0.001	–	–	0.01	0.03	–	–	0.37

Note: CEV indicates the carbon equivalent value, determined by: CEV = C+(Cr+Mo+V)/5+Mn/6+(Ni+Cu)/15.

The mechanical properties of parent materials were determined by standard tensile coupon tests. The steel plates were firstly cut into the desired dimension with a width by the length of 120 mm × 400 mm, and each small piece was then press–braked into cold–formed angle sections with different

profiles. Corner tensile coupons were subsequently machined from the cold–formed corner regions and were tested to obtain the mechanical properties after cold–forming. The shape and dimension of tensile coupons were designed conforming to the requirements of EN ISO 6892–1:2019 [30].

2.1 Flat tensile coupons

Three flat tensile coupons were extracted from each parent steel plate along the rolling direction. The dimension of the flat tensile coupon is shown in Fig. 2 (a). In total, 12 pieces of flat tensile coupons were tested to determine the Young's modulus E_f, yield strength $f_{y,f}$, ultimate tensile strength $f_{u,f}$, ultimate strain $\varepsilon_{u,f}$, and elongation at fraction $\varepsilon_{f,f}$ of parent materials. The flat tensile coupons were labelled by their nominal steel grades and plate thicknesses. For example, 550–6–2 represents the second flat tensile coupon extracted from the 6 mm Q550 parent plate.

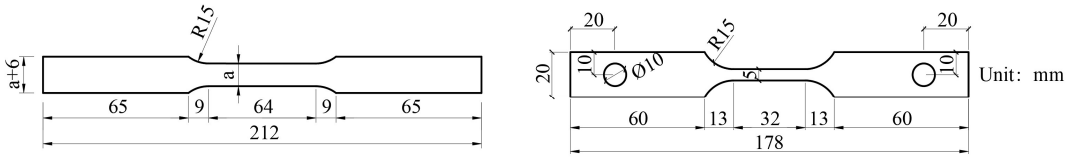

(a) Flat coupon (b) Corner coupon

Fig. 2. Dimensions of flat and corner coupons.

2.2 Corner tensile coupons

As mentioned, the sectioned steel plates were press–braked into cold–formed angle sections with various profiles. The press–braking was performed using a press–braking machine as shown in Fig. 3. To achieve different levels of induced plastic deformation in the corner region of angle sections, various included angles θ of 90°, 120°, 135°, and 150° were designed and different punches with punch radii of 5 mm, 10 mm, and 15 mm were selected in the fabrication process. Profiles of adopted punches are demonstrated in Fig. 4. After cold–forming, the corresponding included angle of specimen was carefully measured using a digital protractor. The tolerance of the included angle set

171 in this study was ± 1° compared to the anticipated angle. Two identical corner tensile coupons were
172 extracted from the same corner region of specimens by a wire cutting machine, while the dimension
173 of corner coupons is illustrated in Fig. 2 (b).

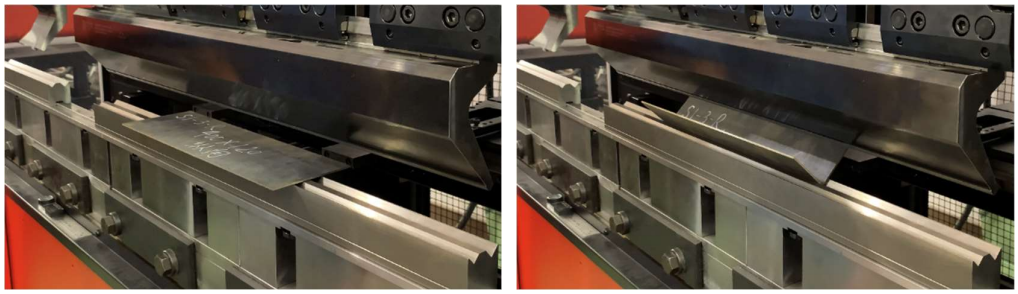
174

175 **Fig. 3**. Fabrication process of the cold–formed angle section.

176

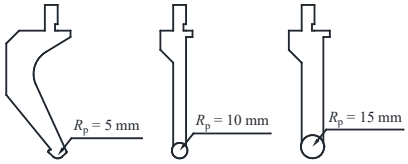

177

178 **Fig. 4**. Geometric profiles of different punches with different punch radii R_p.

179

180 As shown in Fig. 5, each corner coupon's cross–sectional dimension was recorded using a high–
181 resolution scanner, and were subsequently transferred into AutoCAD software for further processing
182 to determine the inner corner radius r_i and cross–sectional area of the parallel length A_c. The specimen
183 label of corner coupons identifies the nominal steel grade, plate thickness, included angle and adopted
184 punch radius. For example, 550–6–135–P15 indicates a corner coupon machined from a 135° angle
185 section fabricated from the 6 mm Q550 parent steel plate using a 15 mm radius punch. It should be
186 noted that some repeated angle specimens were prepared to ensure the repeatability and reliability of
187 the test programme. Therefore, in some cases, four identical corner coupons were machined. Totally,
188 68 corner coupons were tested in this study.

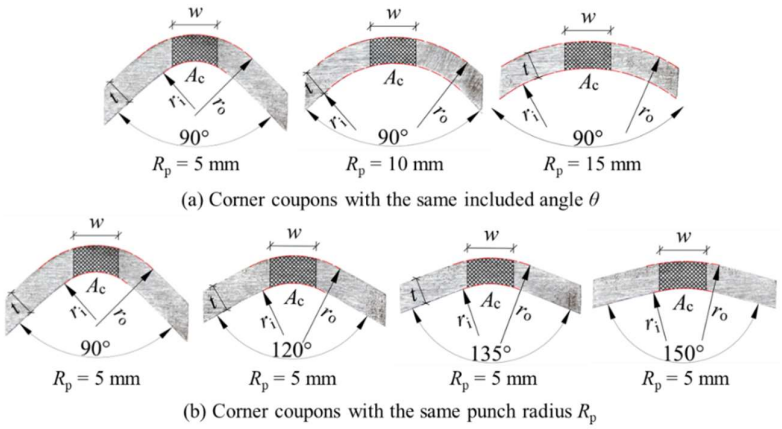

Fig. 5. Processing examples of the corner coupon.

2.3 Tensile coupon test

The stress–strain responses of tensile coupons were obtained using a LABSANS material testing machine. A pair of uniaxial strain gauges and an extensometer (50 mm gauge length for flat coupons and 25 mm gauge length for corner coupons) were mounted on tensile coupons to record the longitudinal strain development. Young's modulus for each coupon was determined through a linear regression of recorded stress over the average reading of strain gauges between the range of $0.1f_y$ to $0.4f_y$. Fig. 6 shows the test apparatus of flat and corner coupon tests, in which flat coupons were gripped using a flat end clamp, while corner coupons were tested using a specially–designed pin grip to diminish the effect of eccentricity. Similar loading procedures used in [3, 31] were adopted, in which initial loading speeds of 0.3 mm/min until 0.2% proof strength, 0.8 mm/min up to the ultimate tensile strength, and 2 mm/min until the fracture of specimens, were used. It is worth noting that before the tensile coupon test, pairs of fine lines with a distance of $5.65\sqrt{(A_c)}$ have been marked on the surface within the parallel length of coupons. The proportional elongation at fracture of specimens can be then obtained by comparing the distance between mark lines after fracture to the original length after carefully fitting the fractured pieces.

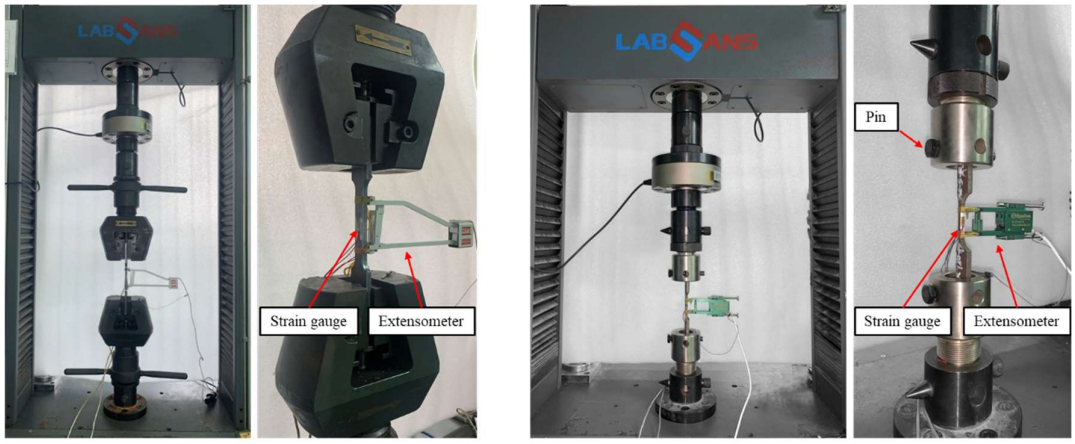

(a) Test setup for flat coupons (b) Test setup for corner coupons

Fig. 6. Test setup for flat and corner coupons.

2.4 Test results

The obtained engineering stress-strain curves are plotted in Fig. 7, in which black and red lines represent the stress-strain curves of parent materials before and after cold-forming. It should be noted that the necking of specimen 460–3–90–P15–1 occurred out of the measurement range of extensometer. Therefore, the recorded elongation after the initiation of necking was much smaller than the actual elongation. The measured mechanical properties of flat and corner tensile coupons, including the Young's modulus E, 0.2% proof strength f_y, ultimate tensile strength f_u, ultimate strain ε_u, and elongation at fraction ε_f are summarised in Table 2 and Table 3, respectively. To distinguish those properties among different sets of coupons, subscripts "f" and "c" were adopted for flat and corner coupons, respectively. The average yield strengths $f_{y,f}$ for 3mm Q460, 6 mm Q460, 6 mm Q550, and 3 mm Q690 steel plates are 520 MPa, 523 MPa, 646 MPa, and 741 MPa, respectively. After cold-forming, the enhanced yield strength $f_{y,c}$ ranges from 562 MPa to 874 MPa.

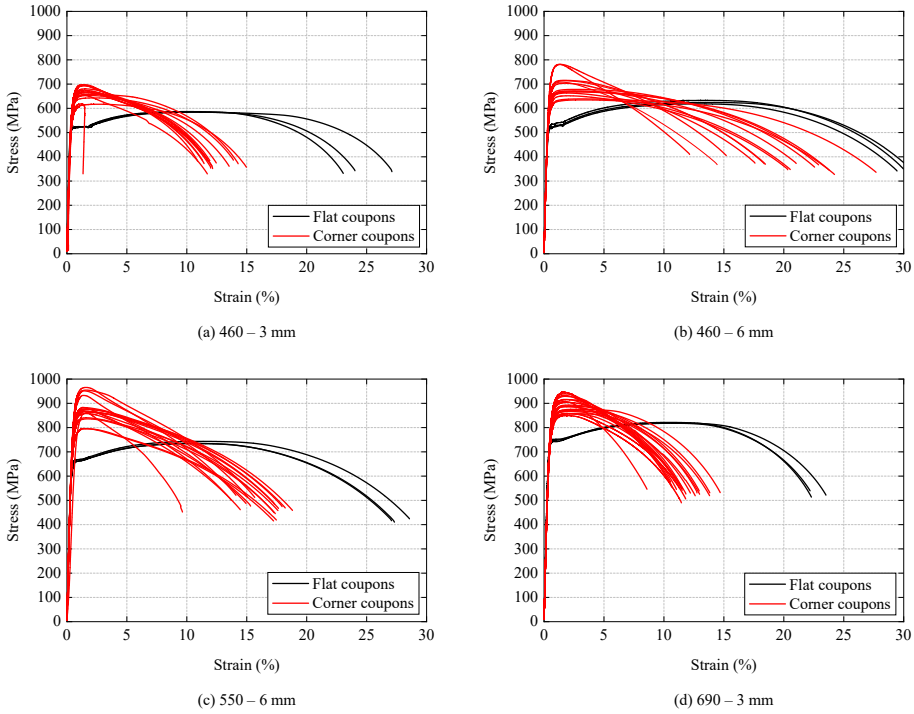

Fig. 7. Stress–strain curves of tested tensile coupons.

Table 2. Summary of key material parameters from flat coupon tests.

Specimen		E_f	$f_{y,f}$	$f_{u,f}$	$\varepsilon_{u,f}$	$\varepsilon_{f,f}$	k	n_{se}
–		(GPa)	(MPa)	(MPa)	(%)	(%)	–	–
460–3	–R1	204	521	587	9.79	23.05	843.2	0.112
	–R2	205	521	585	10.14	27.11	842.0	0.114
	–R3	203	519	584	10.41	24.02	847.7	0.117
	Mean	204	520	585	10.11	24.73	844.3	0.114
460–6	–R1	194	515	618	12.80	29.44	928.6	0.135
	–R2	193	531	633	13.64	29.96	949.2	0.135
	–R3	195	521	624	13.61	30.54	937.7	0.135
	Mean	194	523	625	13.35	29.98	938.5	0.135
550–6	–R1	198	643	734	10.78	27.32	1034.9	0.106
	–R2	199	643	735	10.49	27.66	1036.6	0.106
	–R3	210	652	743	11.36	29.29	1059.9	0.111
	Mean	202	646	737	10.88	28.09	1043.8	0.108
690–3	–R1	201	746	819	11.00	23.51	1147.4	0.103
	–R2	204	743	818	10.56	22.19	1147.5	0.104
	–R3	214	733	821	10.45	22.30	1152.7	0.104
	Mean	206	741	819	10.67	22.67	1149.2	0.104

Table 3. Summary of key material parameters from corner coupon tests.

Specimen		r_i/t	E_c	$f_{y,c}$	$f_{u,c}$	$\varepsilon_{u,c}$	$\varepsilon_{f,c}$	Specimen		r_i/t	E_c	$f_{y,c}$	$f_{u,c}$	$\varepsilon_{u,c}$	$\varepsilon_{f,c}$
–		–	(GPa)	(MPa)	(MPa)	(%)	(%)	–		–	(GPa)	(MPa)	(MPa)	(%)	(%)
460–3–90–P5	–1	1.74	193	636	692	1.41	13.91	550–6–90–P10	–1	1.67	204	803	881	1.41	16.40
	–2	1.78	190	643	697	1.25	14.82		–2	1.67	201	798	871	1.19	16.33
	–3	1.83	199	639	698	1.41	14.05	550–6–90–P15	–1	2.33	199	781	858	1.60	18.03
	–4	1.77	183	636	695	1.41	13.50		–2	2.23	197	789	867	1.67	18.43
460–3–90–P10	–1	3.70	187	606	658	1.94	17.68		–3	2.48	201	767	841	1.63	17.23
	–2	Test failed							–4	2.53	202	759	836	1.82	18.17
460–3–90–P15	–1	5.43	186	562	617	2.59	18.82	550–6–120–P10	–1	Test failed					
	–2	5.54	194	573	618	1.18	16.55		–2	1.53	197	806	881	1.31	16.83
460–3–120–P5	–1	2.64	192	611	667	1.50	15.41	550–6–135–P10	–1	1.80	200	792	867	1.55	17.20
	–2	2.39	187	610	664	1.56	15.18		–2	1.98	201	797	877	1.60	17.83
	–3	2.28	189	623	680	1.53	15.27		–3	1.81	198	794	875	1.64	18.10
	–4	2.23	190	601	654	1.36	15.36		–4	2.03	198	788	867	1.68	19.30
460–3–135–P5	–1	2.55	194	613	668	1.46	17.50	550–6–150–P10	–1	3.18	194	728	795	1.38	18.53
	–2	2.96	193	618	675	1.43	15.86		–2	3.05	195	727	795	1.65	19.00
460–3–150–P5	–1	3.94	194	597	653	1.71	18.05	690–3–90–P5	–1	1.91	193	846	942	1.44	15.77
	–2	4.09	191	606	643	2.23	18.36		–2	1.90	193	845	939	1.74	14.82
460–6–90–P5	–1	0.82	192	718	781	1.40	17.50		–3	1.83	195	833	929	1.75	15.95
	–2	0.73	193	718	782	1.30	16.33		–4	1.89	195	835	933	1.74	16.00
460–6–90–P10	–1	1.66	194	654	708	1.45	18.20	690–3–90–P10	–1	3.73	195	808	887	1.91	15.05
	–2	1.66	194	660	713	1.72	19.40		–2	3.69	193	800	893	2.02	15.91
460–6–90–P15	–1	2.58	194	618	672	2.55	20.17		–3	3.61	194	798	886	1.89	15.68
	–2	2.57	194	624	678	2.77	22.23		–4	3.61	197	800	889	2.06	16.50
	–3	2.55	193	616	668	2.51	22.00	690–3–90–P15	–1	5.60	194	783	868	2.61	19.41
	–4	2.53	200	617	669	2.75	21.90		–2	5.50	197	788	875	2.67	18.36
460–6–120–P10	–1	1.46	195	663	716	1.66	20.60		–3	5.63	193	771	858	2.53	17.27
	–2	1.45	192	651	703	1.73	19.00		–4	5.62	195	770	857	2.21	16.86
460–6–135–P10	–1	2.00	189	599	652	2.02	20.33	690–3–120–P5	–1	2.08	191	817	908	1.67	14.59
	–2	1.94	190	610	663	1.91	20.50		–2	1.97	195	821	916	1.79	15.64
460–6–150–P10	–1	2.89	192	583	635	3.25	25.23	690–3–135–P5	–1	2.57	200	819	915	1.94	15.55
	–2	2.96	195	587	639	3.22	24.17		–2	2.74	200	814	904	1.91	15.45
550–6–90–P5	–1	0.82	195	863	951	1.42	16.53	690–3–150–P5	–1	4.04	196	765	858	1.87	15.45
	–2	0.80	196	844	933	1.33	15.53		–2	3.78	192	760	850	1.82	16.36
	–3	0.75	197	865	955	1.63	15.97		–3	3.86	191	777	866	2.01	15.27
	–4	0.76	198	874	966	1.61	16.13		–4	4.93	192	779	871	2.04	14.64

The strength enhancement level $f_{y,c}/f_{y,f}$ is strongly correlated with the experienced plastic deformation, which was associated with the designed included angle θ and adopted punch radius R_p during the press–braking process. Fig. 8 shows the relationships between the enhanced strengths ($f_{y,c}$ and $f_{u,c}$) and control parameters (θ and R_p). A smaller included angle produces a smaller inner corner radius r_i for specimens press–braked by the same punch, which causes a larger plastic deformation, and, thus, a higher strength enhancement. It is also evident that employing a punch with a smaller punch radius results in a tighter inner corner radius r_i for specimens with the same included angle (take 90° as an example), yielding a more considerable strength enhancement.

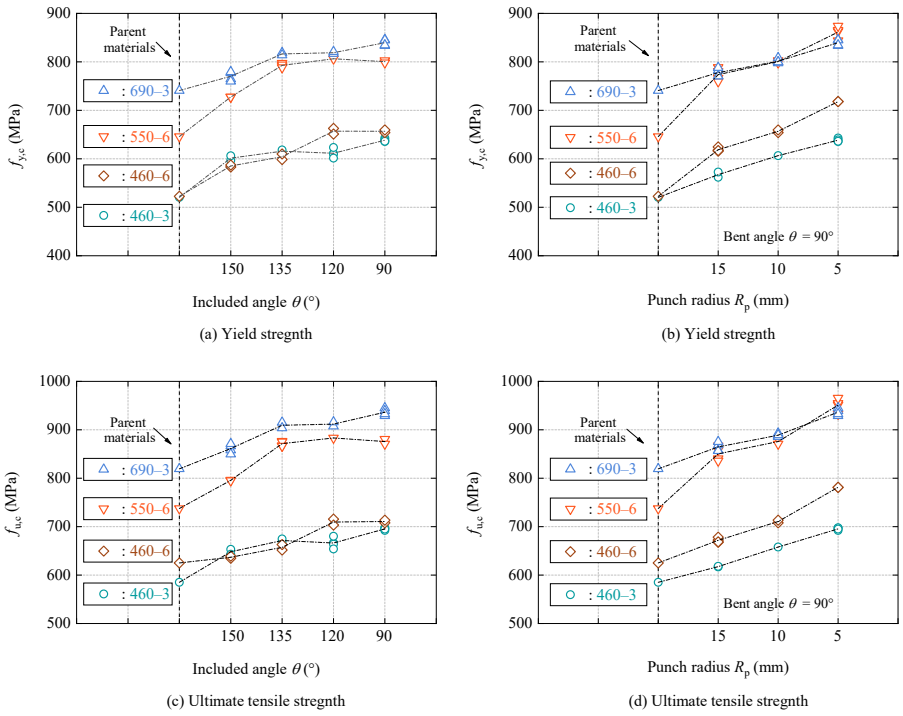

239

240

241 **Fig. 8**. Trends of strengths $f_{y,c}$ and $f_{u,c}$ against various punch radii R_p and included angles θ.

242

243 **3. Development of the cold–formed steel database**

244 To characterise the mechanical properties of cold–formed steels in the corner region, more than
245 900 tensile test results, either generated in this study or published in literature [3, 17, 22, 23, 25-27,
246 32-60], were collated to establish a comprehensive database, which includes test results of 341 flat
247 coupons and 613 corner coupons. The key information of collected material test data is summarised
248 in Table 4, including source, nominal steel grade or yield strength, available material parameters (the
249 Young's modulus E, yield strength f_y, ultimate tensile strength f_u, ultimate strain ε_u, elongation at
250 fraction ε_f, and inner corner radius to thickness ratio r_i/t), number of test data, and cross–section from
251 which the coupons were extracted. It should be noted that some unpublished test data from the authors'
252 research group were also included in the database.

253

Table 4. Information summary of cold–formed steel material test data.

References	Steel grade or yield strength	Cross–sections from which coupons were extracted	Available parameters of flat coupons	Available parameters of corner coupons	Number of data
Normal strength steel					
Liu et al. [3]	Q235/Q275/Q355	Angle sections	$E_f, f_{y,f}, f_{u,f}, \varepsilon_{u,f}, \varepsilon_{f,f}$	$E_c, f_{y,c}, f_{u,c}, \varepsilon_{u,c}, \varepsilon_{f,c}, r_i/t$	143
Gardner et al. [17]	235 MPa	SHS/RHS	$E_f, f_{y,f}, f_{u,f}$	$E_c, f_{y,c}, f_{u,c}, r_i/t$	5
Guo et al. [32]	235 MPa	SHS/RHS	$f_{y,f}, f_{u,f}$	$f_{y,c}, f_{u,c}, r_i/t$	6
Kettler [33]	S275/S355	SHS/RHS	$E_f, f_{y,f}, f_{u,f}$	$f_{y,c}, f_{u,c}, \varepsilon_{u,c}$	2
Singh and Singh [34]	Yst–310	SHS/RHS	$E_f, f_{y,f}, f_{u,f}$	$E_c, f_{y,c}, f_{u,c}, r_i/t$	5
Tayyebi and Sun [35]	344–409 MPa	SHS/RHS	$E_f, f_{y,f}, f_{u,f}$	$E_c, f_{y,c}, f_{u,c}, r_i/t$	5
Key et al. [36]	350 MPa	SHS/RHS	$f_{y,f}, f_{u,f}$	$f_{y,c}, f_{u,c}, \varepsilon_{u,c}, r_i/t$	11
Zhu et al. [37]	355 MPa	SHS/RHS	$E_f, f_{y,f}, f_{u,f}, \varepsilon_{u,f}$	$E_c, f_{y,c}, f_{u,c}, \varepsilon_{u,c}, r_i/t$	2
Liu et al. [38]	Q355	SHS/RHS	$E_f, f_{y,f}, f_{u,f}, \varepsilon_{u,f},$	$E_c, f_{y,c}, f_{u,c}, \varepsilon_{u,c}, r_i/t$	8
Afshan et al. [39]	S355	SHS/RHS	$E_f, f_{y,f}, f_{u,f}$	$E_c, f_{y,c}, f_{u,c}, \varepsilon_{u,c}, r_i/t$	8
Hayeck [40]	S355	RHS	$E_f, f_{y,f}, f_{u,f}$	$f_{y,c}, f_{u,c}, \varepsilon_{u,c}$	12
Hayeck et al. [41]	S355/S460	SHS/RHS	–	$f_{y,c}, f_{u,c}, \varepsilon_{u,c}$	95
Wilkinson and Hancock [42]	C350/C450	SHS/RHS	$f_{y,f}, f_{u,f}$	$f_{y,c}, f_{u,c}, r_i/t$	51
Hui [43]	390 MPa	Channel sections	–	$f_{y,c}, f_{u,c}, \varepsilon_{u,c}$	4
High strength steel					
This study	Q460/Q550/Q690	Angle sections	$E_f, f_{y,f}, f_{u,f}, \varepsilon_{u,f}, \varepsilon_{f,f}$	$E_c, f_{y,c}, f_{u,c}, \varepsilon_{u,c}, \varepsilon_{f,c}, r_i/t$	66
Unpublished data from authors	Q460/Q690	Octagonal hollow sections	$E_f, f_{y,f}, f_{u,f}, \varepsilon_{u,f}, \varepsilon_{f,f}$	$E_c, f_{y,c}, f_{u,c}, \varepsilon_{u,c}, \varepsilon_{f,c}, r_i/t$	23
Pham et al. [22]	G450	Channel sections	$E_f, f_{y,f}, f_{u,f}$	$E_c, f_{y,c}, f_{u,c}, r_i/t$	2
Kyvelou et al. [44]	S450	Channel sections	$f_{y,f}, f_{u,f}$	$f_{y,c}, r_i/t$	2
Liu et al. [38]	Q460	SHS/RHS	$E_f, f_{y,f}, f_{u,f}, \varepsilon_{u,f},$	$E_c, f_{y,c}, f_{u,c}, \varepsilon_{u,c}, r_i/t$	8
Chen et al. [46]	460 MPa	Octagonal hollow sections	$E_f, f_{y,f}, f_{u,f}, \varepsilon_{u,f}, \varepsilon_{f,f}$	$E_c, f_{y,c}, f_{u,c}, \varepsilon_{u,c}, \varepsilon_{f,c}, r_i/t$	8
Li and Young [45]	500 MPa/550 MPa	Built–up cold–formed sections	$E_f, f_{y,f}, f_{u,f}$	$E_c, f_{y,c}, f_{u,c}, r_i/t$	6
Wang et al. [47]	S500/S700/S960	SHS	$f_{y,f}, f_{u,f}$	$f_{y,c}, f_{u,c}, \varepsilon_{u,c}, r_i/t$	9
Tayyebi and Sun [35]	638–730 MPa	SHS/RHS	$E_f, f_{y,f}, f_{u,f}$	$E_c, f_{y,c}, f_{u,c}, r_i/t$	5
Tran et al. [48]	S650	Polugonal hollow sections	–	$f_{y,c}, f_{u,c}, \varepsilon_{u,c}$	6
Liu et al. [49]	Q690	Hexagonal hollow sections	$E_f, f_{y,f}, f_{u,f}$	$E_c, f_{y,c}, f_{u,c}, \varepsilon_{u,c}, r_i/t$	7
Liu et al. [23]	Q690	Irregular hexagonal hollow sections	$E_f, f_{y,f}, f_{u,f}$	$E_c, f_{y,c}, f_{u,c}, \varepsilon_{u,c}, r_i/t$	30
Liu et al. [50]	Q690	Irregular octagonal hollow sections	$E_f, f_{y,f}, f_{u,f}$	$E_c, f_{y,c}, f_{u,c}, \varepsilon_{u,c}, r_i/t$	10
Fang et al. [51]	S690	Octagonal hollow sections	$E_f, f_{y,f}, f_{u,f}$	$E_c, f_{y,c}, f_{u,c}, \varepsilon_{u,c}, r_i/t$	6
Jiang and Zhao [53]	S690	Angle sections	$E_f, f_{y,f}, f_{u,f}$	$E_c, f_{y,c}, f_{u,c}, \varepsilon_{u,c}, r_i/t$	4
Jiang and Zhao [52]	S690	Channel sections	$E_f, f_{y,f}, f_{u,f}$	$E_c, f_{y,c}, f_{u,c}, \varepsilon_{u,c}, r_i/t$	5
Xiao et al. [54]	S690	SHS	$E_f, f_{y,f}, f_{u,f}$	$E_c, f_{y,c}, f_{u,c}, \varepsilon_{u,c}, r_i/t$	6
Zhang et al. [55]	S690	Angle sections	$E_f, f_{y,f}, f_{u,f}$	$E_c, f_{y,c}, f_{u,c}, \varepsilon_{u,c}, r_i/t$	6
Zhang et al. [56]	S690	Channel sections	$E_f, f_{y,f}, f_{u,f}$	$E_c, f_{y,c}, f_{u,c}, \varepsilon_{u,c}, r_i/t$	12
Zhong et al. [57]	S700	SHS	$E_f, f_{y,f}, f_{u,f}$	$E_c, f_{y,c}, f_{u,c}, \varepsilon_{u,c}, r_i/t$	4
Ma et al. [25]	S700/S900	SHS/RHS	$E_f, f_{y,f}, f_{u,f}$	$E_c, f_{y,c}, f_{u,c}, \varepsilon_{u,c}, r_i/t$	11
Yang et al. [58]	S700/S900	SHS	$f_{y,f}, f_{u,f}$	$f_{y,c}, f_{u,c}, \varepsilon_{u,c}, r_i/t$	3
Somodi and Kovesdi [26]	S700/S960	SHS	$f_{y,f}, f_{u,f}$	$f_{y,c}, f_{u,c}, \varepsilon_{u,c}, r_i/t$	3
Pandey and Young [27]	900 MPa/960 MPa	SHS/RHS	$E_f, f_{y,f}, f_{u,f}$	$E_c, f_{y,c}, f_{u,c}, r_i/t$	10
Wang et al. [59]	S960	Angle and channel sections	$E_f, f_{y,f}, f_{u,f}$	$E_c, f_{y,c}, f_{u,c}, \varepsilon_{u,c}, r_i/t$	2
Wang et al. [60]	S960	Channel sections	$E_f, f_{y,f}, f_{u,f}$	$E_c, f_{y,c}, f_{u,c}, \varepsilon_{u,c}, r_i/t$	2
				Total	613

254

As can be seen from Table 4, the assembled database covers a broad spectrum of parameters. The nominal yield strength of the parent structural steel ranges from 235 MPa to 960 MPa, and the measured yield strength of cold–formed corner materials varies from 343 MPa to 1324 MPa. The tensile test results were extracted from various cold–formed cross–sections, including angle sections, channel sections, built–up cold–formed sections, square and rectangular hollow sections, and polygonal hollow sections. In terms of some data extracted from cold–rolled hollow sections, tensile test results of flat coupons machined from flat faces were used to represent the mechanical properties of parent materials. This strategy was considered acceptable since the average strength enhancement of flat materials in cold–rolled hollow sections was only around 4% [17].

Since the material parameters of tensile coupons in different literature were reported in various degrees of completeness, the number of data used for different analyses varies among different sub–groups. Among the 314 flat coupon test results, 209 tests reported their full–range stress–strain curves. These curves were then utilised to establish the relationships between $f_{u,f}/f_{y,f}$ ratio and material coefficient k and strain–hardening exponent n_{se}. These data combined with the remaining flat coupon data also served as the benchmark parameters in the following analysis for cold–formed steels. Among the 613 corner coupon tests, 385 test results were used for deriving the predictive model for the Young's modulus E_c of cold–formed steels, 482 for enhanced yield strength $f_{y,c}$, 472 for enhanced ultimate strength $f_{u,c}$, 514 for ultimate strain $\varepsilon_{u,c}$, and 209 for elongation at fracture $\varepsilon_{f,c}$, respectively. Distributions of r_i/t ratios after cold–forming with respect to parent material yield strengths are plotted in Fig. 9.

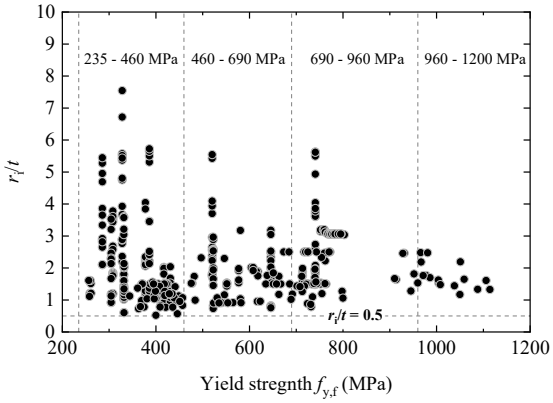

Fig. 9. Distributions of r_i/t ratios after cold–forming with respect to parent material yield strengths in the database.

4. Analysis of results and development of predictive expressions

4.1 Recalibration of material parameters of parent materials

The material coefficient k and the strain–hardening exponent n_{se} were implicitly incorporated in the predictive expression Eq. (2) for predicting the enhanced yield strength. The empirical relationships of k and n_{se} proposed by Karren [12] and Liu et al. [3] were only based on NSS with nominal yield strength no greater than 355 MPa. Hence, to incorporate HSS, full–range stress–strain curves of HSS were used to determine k and n_{se}. The engineering stress–strain responses (σ_E–ε_E) of parent materials were converted to true stress–strain responses (σ_T–ε_T) using Eq. (7) and Eq. (8), and the obtained σ_E–ε_E responses were subsequently plotted on a log–log scale paper. The processing examples for NSS and HSS are depicted in Fig. 10 (a) and (b), respectively.

$$\sigma_T = \sigma_E(1+\varepsilon_E) \tag{7}$$

$$\varepsilon_T = \ln(1+\varepsilon_E) \tag{8}$$

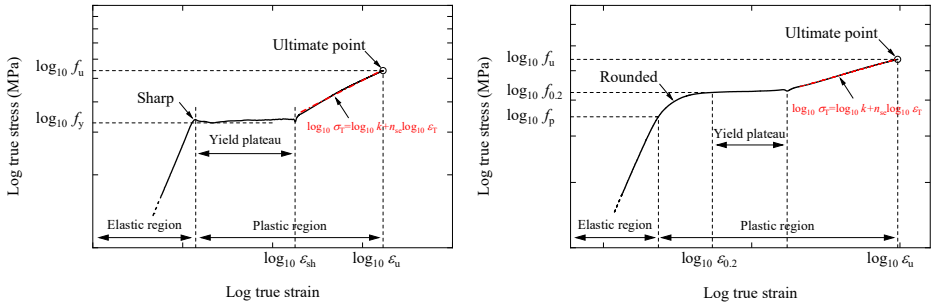

(a) Stress–strain curve of normal strength steel (b) Stress–strain curve of high strength steel

Fig. 10. Processing examples to obtain material coefficient k and strain–hardening exponent n_{se}.

Discarding the elastic range and yield plateau of the stress–strain curves, the correlation between $\log_{10}\sigma_T$ and $\log_{10}\varepsilon_T$ appears as a straight line in the plastic range. Thus, a linear regression analysis using an equation form of Eq. (1) was conducted on the plastic range in line with the procedure described in Karren [12] and Liu et al. [3]. The obtained results of k and n_{se} from all high strength parent materials are given in Table 2, and are plotted with results of NSS in Fig. 11 (a) and (b), respectively. Linear relationships between material parameters and values of $f_{y,f}$ and $f_{u,f}$ were acquired, as expressed in Eq. (9) and Eq. (10). The proposed predictive expressions for k and n_{se} combined with Eq. (1) can provide an accurate representation of stress–strain response of parent material in the plastic range, and link the mechanical properties of parent material to strength enhancement models (discussed in Section 4.2.2).

$$k = 2.630 f_{u,f} - 1.329 f_{y,f} \quad (9)$$

$$n_{se} = 0.262 f_{u,f}/f_{y,f} - 0.175 \quad (10)$$

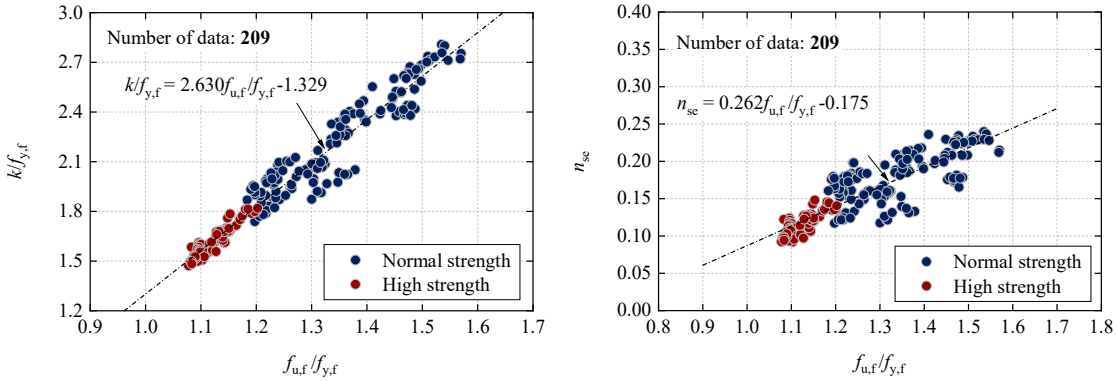

(a) Material coefficient k (b) Strain hardening exponent n_{se}

Fig. 11. Assessment of the material coefficients k and strain hardening exponents n_{se}.

4.2 Cold–formed steels in the corner region

4.2.1 Young's modulus

The average Young's moduli of flat coupon E_f and corner coupon E_c for NSS and HSS are listed in Table 5. The average E_f of parent materials is 207,108 MPa, and the average E_c of cold–formed corner materials is 197,672 MPa, which is 4.4% lower than that of parent materials, indicating that the Young's modulus is slightly reduced due to the experienced plastic deformation [61, 62]. Fig. 12 indicates that generally, no apparent trend can be observed between the reduction of Young's modulus and strength enhancement level. Hence, given the consistent test result, the Young's modulus of cold–formed steels in the corner region may be determined as 197,000 MPa or 95% of that of parent material. It should be noted that the recommended E values for cold–formed steel in the European code [21], American specification [13] and Australian standard [14] are 210,000 MPa, 203,000 MPa, and 200,000 MPa, respectively.

Table 5. Summary of Young's moduli for NSS and HSS.

Materials	Number of data	E_f	E_c	E_c/E_f
		Average value		
	–	MPa	MPa	–
Normal strength steel	170	206,646	194,783	0.945
High strength steel	215	207,475	199,969	0.964
All	385	207,108	197,672	0.956

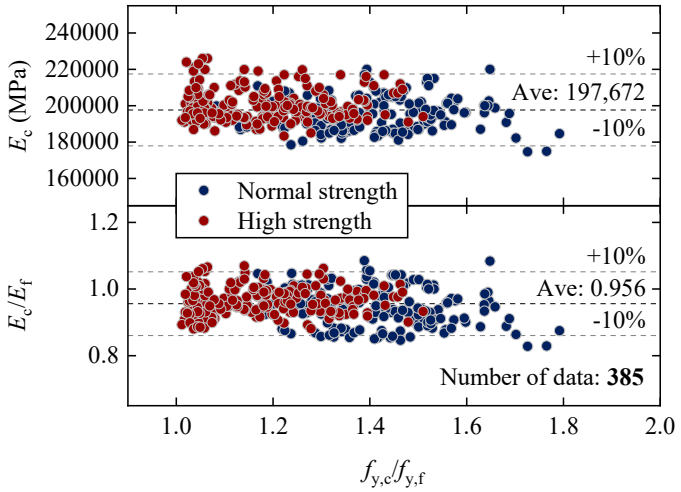

Fig. 12. Trend between the changes in Young's modulus and strength enhancement level.

4.2.2 Strengths

In Fig. 13, the development of f_u/f_y ratios against yield strength f_y for structural steel before and after cold–forming is depicted. A general trend of reducing f_u/f_y ratio with the strength enhancement caused by cold–forming effects can be apparently observed. Moreover, the majority of flat and corner coupon results fulfil the strength ratio requirement ($f_u/f_y > 1.05$) of EN 1993–1–12 [63].

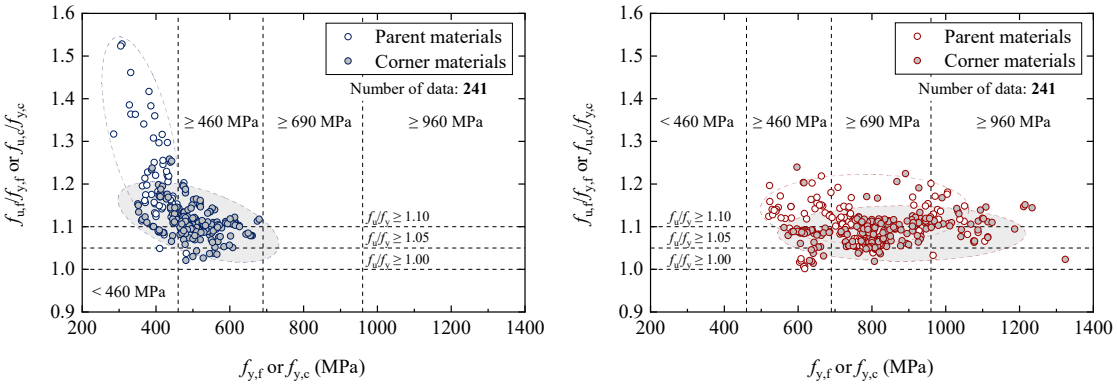

(a) Normal strength steel (b) High strength steel

335

336 **Fig. 13**. Relationships of the f_u/f_y with f_y for NSS and HSS before and after cold–forming.

337

338 The relationships between the strength enhancement levels $f_{y,c}/f_{y,f}$, r_i/t ratios and $f_{u,f}/f_{y,f}$ ratios can

339 be revealed in Fig. 14 (a), in which additional 143 normal strength corner coupon test results from

340 Liu et al. [3] are also plotted for comparison. This figure demonstrates that there is no obvious

341 difference between normal strength and high strength steels in the strength enhancement mechanism.

342 As indicated in Figs. 14 and 15, the strength enhancement behaviour is affected by the $f_{u,f}/f_{y,f}$ ratio of

343 parent materials and the indicator of plastic deformation r_i/t ratio after cold–forming. Also, as shown

344 in Fig. 14 (b), it is worth noting that a similar conclusion can be drawn for the strength enhancement

345 of ultimate tensile strength for normal and highs strength structural carbon steels, which means the

346 relationship of $f_{u,c}/f_{y,f}$, r_i/t, and $f_{u,f}/f_{y,f}$ can also be potentially predicted.

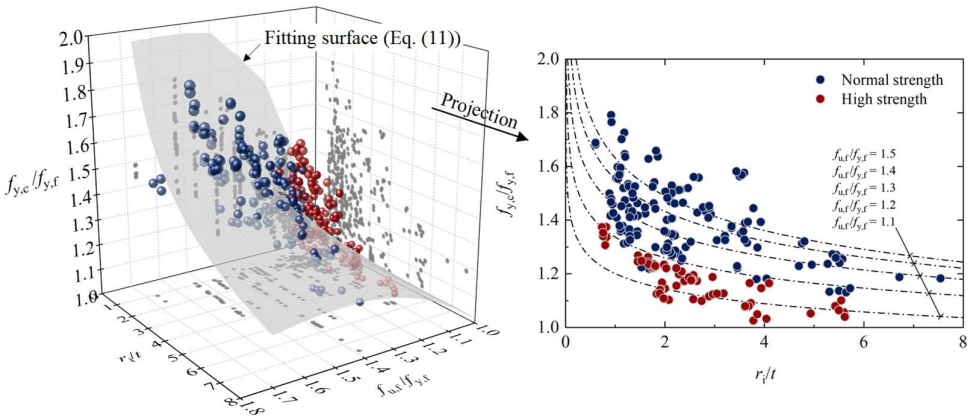

347 (a) Enhanced yield strength $f_{y,c}$ - 3D plot and 2D plot

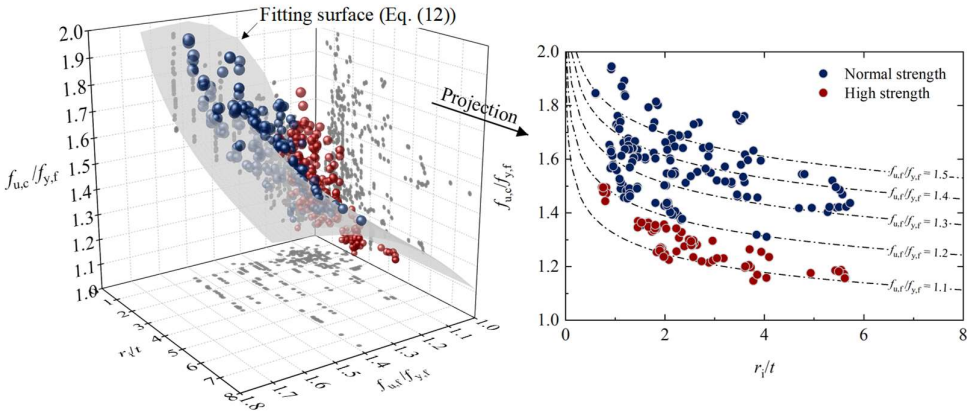

(b) Enhanced ultimate strength $f_{u,c}$ - 3D plot and 2D plot

Fig. 14. Trends of strength enhancement level against r_i/t ratio and $f_{u,f}/f_{y,f}$ ratio.

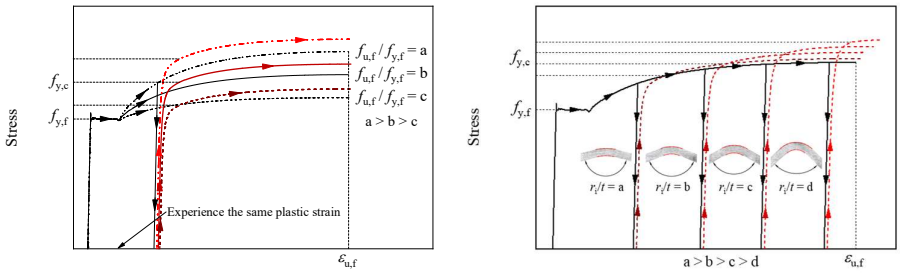

(a) Effect of $f_{u,f}/f_{y,f}$ ratio (b) Effect of r_i/t ratio

Fig. 15. Effects of $f_{u,f}/f_{y,f}$ ratio and r_i/t ratio on the strength enhancement behaviour.

Based on the abovementioned findings, the equations proposed in [3] to predict strength enhancements for the normal strength steel have been adopted to evaluate those behaviours of high strength steel, as shown in Eqs. (11) and (12).

$$f_{y,c}=\frac{B_c f_{y,f}}{\left(r_i/t\right)^{\beta}} \text{ in which } \begin{cases} B_c = 2.769\left(f_{u,f}/f_{y,f}\right)-0.581\left(f_{u,f}/f_{y,f}\right)^2-1.182 \\ \beta = 0.314\left(f_{u,f}/f_{y,f}\right)-0.320 \end{cases} \tag{11}$$

$$f_{u,c}=\frac{B_c f_{y,f}}{\left(r_i/t\right)^{\beta}} \text{ in which } \begin{cases} B_c = 2.807\left(f_{u,f}/f_{y,f}\right)-0.505\left(f_{u,f}/f_{y,f}\right)^2-1.217 \\ \beta = 0.254\left(f_{u,f}/f_{y,f}\right)-0.265 \end{cases} \tag{12}$$

It can be seen from Fig. 16 that the majority of collected data fall within 10% of the predicted value, and all data are within 20%. A similar prediction accuracy may be found for the normal strength

and high strength steel. The mean predicted–to–measured values of enhanced yield strength $f_{y,c}$ and enhanced ultimate strength $f_{u,c}$ are 1.00, 0.99, 1.00, and 1.00 for the normal strength and high strength steel, respectively. Moreover, the prediction accuracy with corresponding coefficient of variation (COV) of those models proposed by Karren [12], Gardner et al. [17] and Rossi et al. [18] are given in Table 6.

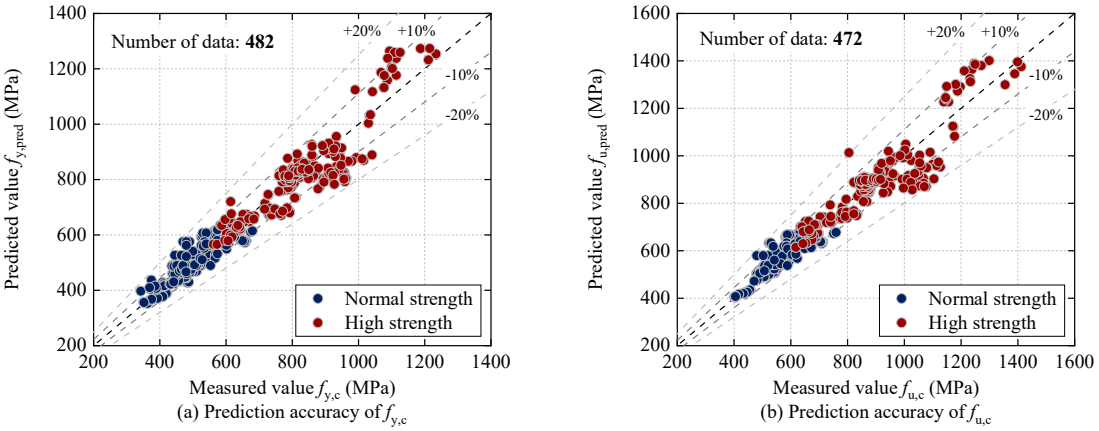

Fig. 16. Prediction accuracy for enhanced yield and ultimate strengths.

Table 6. Comparison results between different predictive expressions.

	Number of data		Predicted-to-measured values			
			Proposed model [3]	Karren's model [12]	Gardner's model [17]	Rossi's model [18]
$f_{y,c}$ (NSS)	241	Mean	1.00	1.08	0.91	0.94
		COV	0.064	0.079	0.123	0.060
$f_{y,c}$ (HSS)	241	Mean	0.99	1.00	0.89	0.96
		COV	0.072	0.073	0.085	0.052
$f_{u,c}$ (NSS)	231	Mean	1.00	–	–	–
		COV	0.051	–	–	–
$f_{u,c}$ (HSS)	241	Mean	1.00	–	–	–
		COV	0.077	–	–	–

4.2.3 Ultimate strain

The ultimate strain of corner coupons was found to be gradually reduced with the increase of cold–works. To make a direct comparison, the corner coupon test results of NSS from Liu et al. [3]

and HSS generated in this study are presented in Fig. 17 (a), in which the values of $\varepsilon_{u,c}/\varepsilon_{u,f}$ (the ultimate strains after and before cold–forming) are plotted against the strength enhancement level $f_{y,c}/f_{y,f}$. It can be seen from Fig. 17 (a) that HSS may suffer severer deterioration on ultimate strain after cold–forming as compared with NSS, which may be attributed to the lower $f_{u,f}/f_{y,f}$ ratio of parent materials. Based on a process of regression analysis, a predictive expression for $\varepsilon_{u,c}$ was proposed and expressed as Eq. (13), in which the effects of $f_{u,f}/f_{y,f}$ of parent materials were directly incorporated.

$$\varepsilon_{u,c} / \varepsilon_{u,f} = \frac{\left[-6.093 + 5.727(f_{u,f} / f_{y,f})\right]}{(f_{y,c} / f_{y,f})^{\left[18.594 - 7.602(f_{u,f}/f_{y,f})\right]}} + 0.059, \text{ but } \varepsilon_{u,c} / \varepsilon_{u,f} \le 1.0 \text{ for } \varepsilon_{u,f} \text{ is available} \quad (13)$$

Moreover, suppose the original ultimate strain $\varepsilon_{u,f}$ of parent material is not reported. In that case, the corner coupon yield and ultimate strength are known (or can be predicted using Eq. (11) and Eq. (12)). A predictive expression for $\varepsilon_{u,c}$ without using $\varepsilon_{u,f}$ is preferred. Hence, the collected 516 ultimate strain values in the developed database are also plotted against the corresponding $f_{u,c}/f_{y,c}$ ratios in Fig. 17 (b). In the same figure, a best-fitting curve with its 95% prediction band is presented and the fitting curve can be expressed in Eq. (14). Table 7 provides the assessment results for these predictive expressions, with mean values of 1.05 and 1.00, and corresponding COVs of 0.253 and 0.423 for Eq. (13) and Eq. (14), respectively. It should be noted that the ultimate strain of cold–formed steels in the corner region is much lower than that in the flat region and hot–rolled steel, which is similar to the finding presented by Gardner and Yun [29].

$$\varepsilon_{u,c} = 0.01(f_{u,c} / f_{y,c})^{(28 f_{u,c}/f_{y,c} - 25.4)}, \text{ for } \varepsilon_{u,f} \text{ is unavailable} \quad (14)$$

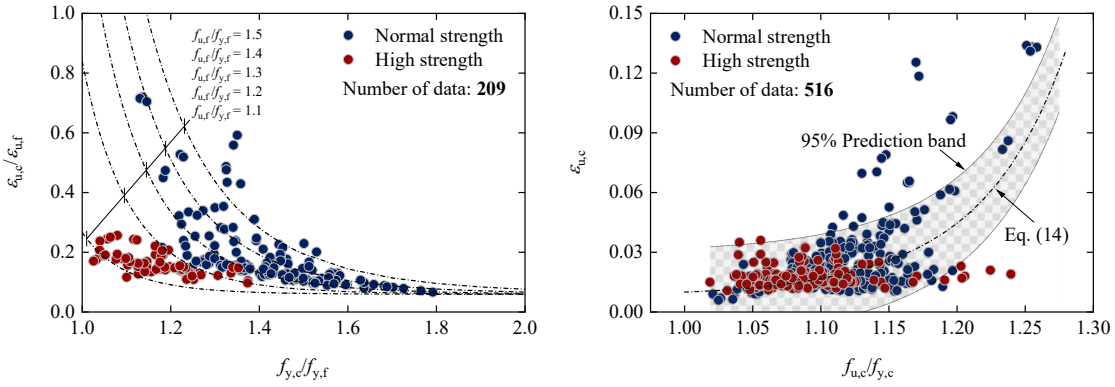

(a) $\varepsilon_{u,f}$ is available (b) $\varepsilon_{u,f}$ is unavailable

393

394 **Fig. 17**. Trend between the change of ultimate strain and related parameters.

395 **Table 7**. Assessment of prediction accuracy for ultimate strain and elongation at fracture.

		Predicted-to-measured values		
		Eq. (13)	Eq. (14)	Eq. (15)
$\varepsilon_{u,c}$ (NSS)	Mean	1.08	1.00	–
	COV	0.238	0.443	–
$\varepsilon_{u,c}$ (HSS)	Mean	0.96	1.00	–
	COV	0.269	0.395	–
$\varepsilon_{u,c}$ (All)	Mean	1.05	1.00	–
	COV	0.253	0.423	–
$\varepsilon_{f,c}$ (NSS)	Mean	–	–	0.98
	COV	–	–	0.190
$\varepsilon_{f,c}$ (HSS)	Mean	–	–	1.06
	COV	–	–	0.107
$\varepsilon_{f,c}$ (All)	Mean	–	–	1.00
	COV	–	–	0.170

396

397 *4.2.4 Elongation at fracture*

398 Elongation at fracture is indicative of the plastic deformation that steel can undergo before
399 fracture. Since most of the elongations at fracture $\varepsilon_{f,c}$ were not reported in the literature and not all of
400 them were measured in a standard manner, only the NSS data from Liu et al. [3] and the HSS data
401 from this study were used in this study to make a consistent comparison. The elongation at fracture
402 of corner coupons $\varepsilon_{f,c}$ is normalised by the elongation at fracture of parent materials $\varepsilon_{f,f}$, and plotted
403 against the strength enhancement level in Fig. 18. On the basis of the least square regression analysis,

the proposed predictive expression for $\varepsilon_{f,c}$ is given by Eq. (15) and is plotted with its 95% prediction band in Fig. 18. As reported in Table 7, the mean predicted–to–measured value equals 1.00, with a moderate COV of 0.17.

$$\varepsilon_{f,c}/\varepsilon_{f,f} = 0.202 + 0.779\left(f_{y,c}/f_{y,f}\right)^{-2.914} \quad (15)$$

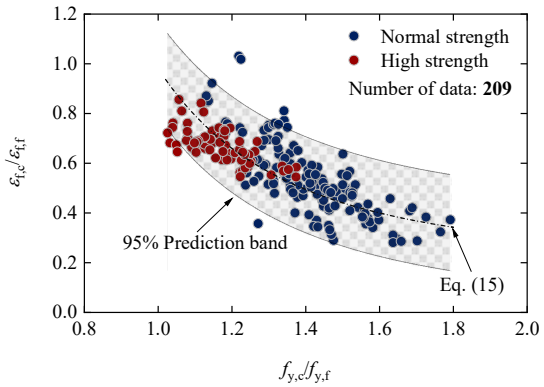

Fig. 18. Trend between the changes in elongation at fracture and strength enhancement level.

5. Summary of proposed predictive expressions

Based on the proposed predictive expressions, the key material parameters of cold–formed normal strength and high strength steels in the corner region may be obtained through the fundamental material parameters of parent materials and geometric dimensions of cold–formed corners. It should be noted that proposed predictive models in this study are applicable to the structural carbon steel when the nominal yield strength of parent materials $f_{y,f}$ ranges from 235 MPa to 960 MPa, the r_i/t value of cold–formed corners varies from 0.5 to 8.0, and the corner included angles ranges from 90° to 150°. The proposed predictive expressions are summarised below.

The Young's modulus E_c of cold–formed steels in the corner region may be taken as 197,000 MPa or 95% of the Young's modulus E_f of parent materials.

Enhanced yield strength $f_{y,c}$ may be determined from:

422 $$f_{y,c}=\frac{B_c f_{y,f}}{\left(r_i/t\right)^{\beta}} \text{ in which } \begin{cases} B_c=2.769\left(f_{u,f}/f_{y,f}\right)-0.581\left(f_{u,f}/f_{y,f}\right)^2-1.182 \\ \beta=0.314\left(f_{u,f}/f_{y,f}\right)-0.320 \end{cases} \quad (16)$$

423 Enhanced ultimate tensile strength $f_{u,c}$ may be obtained from:

424 $$f_{u,c}=\frac{B_c f_{y,f}}{\left(r_i/t\right)^{\beta}} \text{ in which } \begin{cases} B_c=2.807\left(f_{u,f}/f_{y,f}\right)-0.505\left(f_{u,f}/f_{y,f}\right)^2-1.217 \\ \beta=0.254\left(f_{u,f}/f_{y,f}\right)-0.265 \end{cases} \quad (17)$$

425 The ultimate strain $\varepsilon_{u,c}$ may be predicted using Eq. (18) if $\varepsilon_{u,f}$ is available. Otherwise, $\varepsilon_{u,c}$ may

426 be estimated from Eq. (19).

427 $$\varepsilon_{u,c}/\varepsilon_{u,f}=\frac{\left[-6.093+5.727(f_{u,f}/f_{y,f})\right]}{(f_{y,c}/f_{y,f})^{\left[18.594-7.602(f_{u,f}/f_{y,f})\right]}}+0.059, \text{ but } \varepsilon_{u,c}/\varepsilon_{u,f}\le 1.0 \text{ for } \varepsilon_{u,f} \text{ is available} \quad (18)$$

428 $$\varepsilon_{u,c}=0.01(f_{u,c}/f_{y,c})^{(28f_{u,c}/f_{y,c}-25.4)}, \text{ for } \varepsilon_{u,f} \text{ is unavailable} \quad (19)$$

429 Elongation at fraction $\varepsilon_{f,c}$ may be calculated from the following expression:

430 $$\varepsilon_{f,c}/\varepsilon_{f,f}=0.202+0.779\left(f_{y,c}/f_{y,f}\right)^{-2.914} \quad (20)$$

431

432 **6. Conclusion**

433 A comprehensive investigation into the cold–forming effect of normal strength to high strength

434 structural carbon steel has been presented herein. An experimental programme on the cold-forming

435 effect of high strength steel was first carried out. Four types of high strength steel plates were press–

436 braked into the cold–formed angle sections. Tensile tests were conducted on 12 flat coupons extracted

437 from parent materials and 68 corner coupons machined from cold–formed corners. An extensive

438 database comprising more than 900 tensile test results was established based on the obtained test

439 results and collected data from the global literature. Predictive expressions for the key material

440 parameters of cold–formed steels in the corner region have been derived based on the analysis of the

441 developed database. According to the statistical results, the predicted material parameters are shown

442 to be in great agreement with test results. This paper extends the scope of the strength enhancement

443 equation in current north American cold-formed steel design code AISI S100-16 to high strength

steels with grade up to 960 MPa, and provides key predictive material equations that can be further used in the design or numerical modelling of cold-formed steel structures.

Author statement

Haixin Liu: Conceptualisation, Investigation, Methodology, Data curation, Formal analysis, Writing – original draft. **Junbo Chen**: Conceptualisation, Investigation, Methodology, Data curation, Formal analysis, Writing – review & editing. **Tak-Ming Chan**: Methodology, Supervision, Resources, Funding acquisition, Writing – review & editing.

Data availability

Data will be made available on request

Declaration of competing interest

None.

Acknowledgements

The authors are grateful to Dr Xiang Yun for his kind provision of the corner coupon database. The research work presented in this paper was supported by the Research Grants Council of the Hong Kong Special Administrative Region, China (Project No. 15217119). Financial support from Chinese National Engineering Research Centre for Steel Construction (Hong Kong Branch) was also greatly appreciated.

References

[1] G.-C. Li, B.-W. Chen, B.-W. Zhu, Z.-J. Yang, H.-B. Ge, Y.-P. Liu, Axially loaded square concrete-filled steel tubular long columns made of high-strength materials: Experimental investigation, analytical behavior and design, Journal of Building Engineering 58 (2022) 104994.

[2] M.-X. Xiong, P.-W. Pi, W. Gong, M.-F. Yang, Z.-F. Ou, Mechanical properties of TMCP high strength steels with different strength grades at elevated temperatures, Journal of Building Engineering 48 (2022) 103874.

[3] H. Liu, J. Chen, T.-M. Chan, Predictive models for material properties of cold-formed conventional steels in the corner region, Thin-Walled Structures 187 (2023) 110740.

[4] A. Chajes, S. Britvec, G. Winter, Effects of cold-straining on structural sheet steels, Journal of the Structural Division 89(2) (1963) 1-32.

[5] W.F. Hosford, Iron and Steel, Cambridge: Cambridge University Press.2012.

[6] J.-J. Lim, Y.-H. Kim, T.-S. Eom, Compressive strength of high strength concrete-encased composite columns with noncompact and slender steel angles, Journal of Building Engineering 51 (2022) 104341.

[7] A. El Hady, M. El Aghoury, S. Ibrahim, E. Amoush, Experimental investigation of steel built-up beam-columns composed of tracks and channels cold-formed sections, Journal of Building Engineering 51 (2022) 104295.

[8] M. Sifan, P. Gatheeshgar, S. Navaratnam, B. Nagaratnam, K. Poologanathan, J. Thamboo, T. Suntharalingam, Flexural behaviour and design of hollow flange cold-formed steel beam filled with lightweight normal and lightweight high strength concrete, Journal of Building Engineering 48 (2022) 103878.

[9] P. Gatheeshgar, K. Poologanathan, S. Gunalan, K.D. Tsavdaridis, B. Nagaratnam, E. Iacovidou, Optimised cold-formed steel beams in modular building applications, Journal of Building Engineering 32 (2020) 101607.

[10] J. Wang, W. Wang, Y. Xiao, L. Guo, Cyclic behavior tests and evaluation of CFS truss composite floors, Journal of Building Engineering 35 (2021) 101974.

[11] X. Wang, W. Wei, N. Wenchao, Study on the load-carrying capacity of an innovative cold-formed steel floor system, Journal of Building Engineering (2023) 105819.

[12] K.W. Karren, Corner properties of cold-formed steel shapes, Journal of the Structural Division 93(1) (1967) 401-432.

[13] AISI, AISI S100-16. North American Specification for the Design of Cold-Formed Steel Structural Members, American Iron and Steel Institute, The United States, 2016.

[14] AS/NZS, AS/ NZS 4600:2018, Cold-formed steel structures, Standards Australia limited, Australia, 2018.

[15] N. Abdel-Rahman, K. Sivakumaran, Material properties models for analysis of cold-formed steel members, Journal of Structural Engineering 123(9) (1997) 1135-1143.

[16] R.B. Cruise, L. Gardner, Strength enhancements induced during cold forming of stainless steel sections, Journal of Constructional Steel Research 64(11) (2008) 1310-1316.

[17] L. Gardner, N. Saari, F. Wang, Comparative experimental study of hot-rolled and cold-formed rectangular hollow sections, Thin-Walled Structures 48(7) (2010) 495-507.

[18] B. Rossi, S. Afshan, L. Gardner, Strength enhancements in cold-formed structural sections — Part II: Predictive models, Journal of Constructional Steel Research 83 (2013) 189-196.

[19] H.G. Rasmussen KJR, Design of cold-formed stainless steel tubular members. I:columns, Journal of Structural Engineering 119(8) (1993) 2349–2367.

[20] D. Dubina, V. Ungureanu, R. Landolfo, Design of cold-formed steel structures, ECCS – European Convention for Constructional Steelwork, 2012.

[21] CEN, Eurocode 3 - Design of steel structures - Part 1-3: General rules - Supplementary rules for cold-formed members and sheeting, European Committee for Standardization, Brussels, 2006.

[22] C.H. Pham, H.N. Trinh, G. Proust, Effect of manufacturing process on microstructures and mechanical properties, and design of cold-formed G450 steel channels, Thin-Walled Structures 162 (2021).

[23] J.-z. Liu, H. Fang, T.-M. Chan, Experimental investigations on material properties and stub column behaviour of high strength steel irregular hexagonal hollow sections, Journal of Constructional Steel Research 196 (2022).

[24] M. Xiao, Structural behaviour of high strength S690 cold-formed square hollow sections under compression, The Hong Kong Polytechnic University, 2021.

[25] J.-L. Ma, T.-M. Chan, B. Young, Material properties and residual stresses of cold-formed high strength steel hollow sections, Journal of Constructional Steel Research 109 (2015) 152-165.

[26] B. Somodi, B. Kövesdi, Flexural buckling resistance of cold-formed HSS hollow section members, Journal of Constructional Steel Research 128 (2017) 179-192.

[27] M. Pandey, B. Young, Tests of cold-formed high strength steel tubular T-joints, Thin-Walled Structures 143 (2019).

[28] W.M. Quach, J.F. Huang, Stress-Strain Models for Light Gauge Steels, Procedia Engineering 14 (2011) 288-296.

[29] L. Gardner, X. Yun, Description of stress-strain curves for cold-formed steels, Construction and Building Materials 189 (2018) 527-538.

[30] CEN, EN ISO 6892-1:2019. Metallic materials — Tensile testing Part 1: Method of test at room temperature, European Committee for Standardization, Brussels, 2019.

[31] Y. Huang, B. Young, The art of coupon tests, Journal of Constructional Steel Research 96 (2014)

159-175.

[32] Y.-J. Guo, A.-Z. Zhu, Y.-L. Pi, F. Tin-Loi, Experimental study on compressive strengths of thick-walled cold-formed sections, Journal of Constructional Steel Research 63(5) (2007) 718-723.

[33] M. Kettler, Elastic-plastic cross-sectional resistance of semi-compact H-and hollow sections, Graz University of Technology, 2008.

[34] T.G. Singh, K.D. Singh, Experimental investigation on performance of perforated cold–formed steel tubular stub columns, Thin-Walled Structures 131 (2018) 107-121.

[35] K. Tayyebi, M. Sun, Stub column behaviour of heat-treated and galvanized RHS manufactured by different methods, Journal of Constructional Steel Research 166 (2020) 105910.

[36] P.W. Key, S.W. Hasan, G.J. Hancock, Column behavior of cold-formed hollow sections, Journal of Structural Engineering 114(2) (1988) 390-407.

[37] J.-Y. Zhu, T.-M. Chan, B. Young, Cross-sectional capacity of octagonal tubular steel stub columns under uniaxial compression, Engineering Structures 184 (2019) 480-494.

[38] H. Liu, H. Jiang, Y.-F. Hu, T.-M. Chan, K.-F. Chung, Structural behaviour of Q355 and Q460 press-braked rectangular hollow section stub columns, Journal of Constructional Steel Research 197 (2022) 107497.

[39] S. Afshan, B. Rossi, L. Gardner, Strength enhancements in cold-formed structural sections — Part I: Material testing, Journal of Constructional Steel Research 83 (2013) 177-188.

[40] M. Hayeck, Development of a new design method for steel hollow section members resistance, Université de Liège, Liège, Belgique, 2016.

[41] H. Marielle, S. Elsy, N. Joanna, B. Nicolas, Influence of material law on the F.E. modelling of cold-formed tubes, Eighth International Conference on Advances in Steel Structures, Lisbon, Portugal, 2015.

[42] T. Wilkinson, G.J. Hancock, Tests to examine compact web slenderness of cold-formed RHS, Journal of Structural Engineering 124(10) (1998) 1166-1174.

[43] C. Hui, Moment redistribution in cold-formed steel purlin systems, Imperial College London London, 2014.

[44] P. Kyvelou, L. Gardner, D.A. Nethercot, Testing and Analysis of Composite Cold-Formed Steel and Wood−Based Flooring Systems, Journal of Structural Engineering 143(11) (2017) 04017146.

[45] Q.-Y. Li, B. Young, Experimental and numerical investigation on cold-formed steel built-up section pin-ended columns, Thin-Walled Structures 170 (2022).

[46] J. Chen, H. Liu, T.-M. Chan, Material properties and residual stresses of cold-formed octagonal hollow sections, Journal of Constructional Steel Research 170 (2020) 106078.

[47] J. Wang, S. Afshan, N. Schillo, M. Theofanous, M. Feldmann, L. Gardner, Material properties and compressive local buckling response of high strength steel square and rectangular hollow sections,

571 Engineering Structures 130 (2017) 297-315.

572 [48] A.T. Tran, M. Veljkovic, C. Rebelo, L.S. da Silva, Resistance of cold-formed high strength steel
573 circular and polygonal sections — Part 1: Experimental investigations, Journal of Constructional
574 Steel Research 120 (2016) 245-257.

575 [49] J.-z. Liu, H. Fang, S. Chen, T.-M. Chan, Material properties and residual stresses of high strength
576 steel hexagonal hollow sections, Journal of Constructional Steel Research 190 (2022).

577 [50] J.-z. Liu, H. Fang, T.-M. Chan, Experimental and numerical investigations on stub column
578 behaviour of cold-formed high strength steel irregular octagonal hollow sections, Thin-Walled
579 Structures 180 (2022).

580 [51] H. Fang, T.-M. Chan, B. Young, Material properties and residual stresses of octagonal high
581 strength steel hollow sections, Journal of Constructional Steel Research 148 (2018) 479-490.

582 [52] K. Jiang, O. Zhao, Testing, numerical modelling and design of S690 high strength steel channel-
583 to-plate connections, Thin-Walled Structures 179 (2022).

584 [53] K. Jiang, O. Zhao, Net Section Failure of S690 High-Strength Steel Angle-to-Plate Connections,
585 Journal of Structural Engineering 148(4) (2022) 04022021.

586 [54] M. Xiao, Y.F. Hu, M.H. Shen, K.F. Chung, D.A. Nethercot, Compression tests on stocky and
587 slender columns of high strength S690 cold-formed square tubes, Engineering Structures 273 (2022).

588 [55] L. Zhang, F. Wang, Y. Liang, O. Zhao, Press-braked S690 high strength steel equal-leg angle and
589 plain channel section stub columns: Testing, numerical simulation and design, Engineering Structures
590 201 (2019).

591 [56] L. Zhang, F. Wang, Y. Liang, O. Zhao, Experimental and numerical studies of press-braked S690
592 high strength steel channel section beams, Thin-Walled Structures 148 (2020).

593 [57] Y. Zhong, Y. Sun, K. Hai Tan, O. Zhao, Testing, modelling and design of high strength concrete-
594 filled high strength steel tube (HCFHST) stub columns under combined compression and bending,
595 Engineering Structures 241 (2021).

596 [58] L. Yang, F. Yin, J. Wang, A. Bilal, A.H. Ahmed, M. Lin, Local buckling resistances of cold-
597 formed high-strength steel SHS and RHS with varying corner radius, Thin-Walled Structures 172
598 (2022).

599 [59] F. Wang, O. Zhao, B. Young, Testing and numerical modelling of S960 ultra-high strength steel
600 angle and channel section stub columns, Engineering Structures 204 (2020).

601 [60] F. Wang, O. Zhao, B. Young, Flexural behaviour and strengths of press-braked S960 ultra-high
602 strength steel channel section beams, Engineering Structures 200 (2019).

603 [61] J. Liao, X. Xue, M.-G. Lee, F. Barlat, G. Vincze, A.B. Pereira, Constitutive modeling for path-
604 dependent behavior and its influence on twist springback, International Journal of Plasticity 93 (2017)
605 64-88.

606 [62] J. Lin, Y. Hou, J. Min, H. Tang, J.E. Carsley, T.B. Stoughton, Effect of constitutive model on
607 springback prediction of MP980 and AA6022-T4, International Journal of Material Forming 13 (2020)
608 1-13.

609 [63] CEN, Eurocode 3: Design of steel structures -Part 1-12: additional rules for the extension of EN
610 1993 up to steel grades S700, European Committee for Standardization, Brussels, 2007.
611